Special Issue Review Article

NMR IN BIOMEDICINE

Received: 31 August 2009, Revised: 5 January 2010, Accepted: 6 January 2010, Published online in Wiley Online Library: 19 May 2010

(wileyonlinelibrary.com) DOI:10.1002/nbm.1518

MRI quantification of non-Gaussian water diffusion by kurtosis analysis†

Jens H. Jensen[a,b]* and Joseph A. Helpern[a,b,c,d]

Quantification of non-Gaussianity for water diffusion in brain by means of diffusional kurtosis imaging (DKI) is reviewed. Diffusional non-Gaussianity is a consequence of tissue structure that creates diffusion barriers and compartments. The degree of non-Gaussianity is conveniently quantified by the diffusional kurtosis and derivative metrics, such as the mean, axial, and radial kurtoses. DKI is a diffusion-weighted MRI technique that allows the diffusional kurtosis to be estimated with clinical scanners using standard diffusion-weighted pulse sequences and relatively modest acquisition times. DKI is an extension of the widely used diffusion tensor imaging method, but requires the use of at least 3 b-values and 15 diffusion directions. This review discusses the underlying theory of DKI as well as practical considerations related to data acquisition and post-processing. It is argued that the diffusional kurtosis is sensitive to diffusional heterogeneity and suggested that DKI may be useful for investigating ischemic stroke and neuropathologies, such as Alzheimer's disease and schizophrenia. Copyright © 2010 John Wiley & Sons, Ltd.

Keywords: diffusion; non-Gaussian; brain; MRI; kurtosis; DKI; DTI

INTRODUCTION

Molecular diffusion is a random process and, as such, it may be described by probability distributions. The most basic of these is the probability of a molecule moving a given displacement over a given time interval. For simple, homogeneous liquids (e.g. a glass of water), this displacement probability distribution function (PDF) is Gaussian (1), and the diffusion is referred to as Gaussian diffusion. However, in many biological tissues including brain, the presence of barriers (e.g. cell membranes) and compartments (e.g. intracellular and extracellular spaces) alter the water diffusion PDF so that it is, in general, no longer precisely Gaussian and the diffusion is referred to as non-Gaussian. Quantification of the degree of diffusional non-Gaussianity can be useful in characterizing the associated tissue structures on which the PDF depends.

The kurtosis is a dimensionless statistical metric for quantifying the non-Gaussianity of an arbitrary probability distribution (2). If M_n is the nth moment of a distribution about its mean value, then the kurtosis may be defined as

$$K = \frac{M_4}{M_2^2} - 3. \quad (1)$$

For any Gaussian distribution, $K = 0$. If a distribution has less weight on its center and tails compared to a Gaussian with the same variance, then $K < 0$, and if the distribution has more weight on its center and tails, then $K > 0$. One can prove the general lower bound $K \geq -2$.

Recently, it has been shown how to estimate, in brain, the kurtosis of the water diffusion displacement PDF with relatively simple diffusion-weighted imaging protocols that are suitable for clinical MRI systems (3–5). This method has been referred to as diffusional kurtosis imaging (DKI) and is a natural extension of diffusion tensor imaging (DTI) (6–10). With DKI, one obtains estimates for all the standard DTI diffusion metrics, such as the mean diffusivity (MD) and the fractional anisotropy (FA), and also for several additional metrics related to the diffusional kurtosis. In this way, DKI provides for a more complete characterization of water diffusion in brain. Here we review both the underlying theory of DKI and practical aspects of its implementation.

* *Correspondence to: J. H. Jensen, Department of Radiology, New York University School of Medicine, 660 First Avenue, 4th Floor, New York, NY 10016–3295, USA.*
E-mail: jj33@nyu.edu

a *J. H. Jensen, J. A. Helpern*
Center for Biomedical Imaging, Department of Radiology, New York University School of Medicine, New York, New York

b *J. H. Jensen, J. A. Helpern*
Department of Physiology and Neuroscience, New York University School of Medicine, New York, New York

c *J. A. Helpern*
Department of Psychiatry, New York University School of Medicine, New York, New York

d *J. A. Helpern*
Center for Advanced Brain Imaging, Nathan S. Kline Institute for Psychiatric Research, Orangeburg, New York

Contract/grant sponsor: National Institutes of Health; contract/grant numbers; 1R01AG027852 and 1R01EB007656.
Contract/grant sponsor: Litwin Foundation for Alzheimer's Research.
Contract/grant sponsor: Werner Dannheisser Trust.
Contract/grant sponsor: Institute for the Study of Aging.

† *This article is published in NMR in Biomedicine as a special issue on Progress in Diffusion-Weighted Imaging: Concepts, Techniques, and Applications to the Central Nervous System, edited by Jens H. Jensen and Joseph A. Helpern, Center for Biomedical Imaging, Department of Radiology, NYU School of Medicine, New York, NY, USA.*

Abbreviations used: *CSF, cerebrospinal fluid; DKI, diffusional kurtosis imaging; DTI, diffusion tensor imaging; FA, fractional anisotropy; FWM, frontal white matter; GM, gray matter; GP, globus pallidus; GRAPPA, generalized autocalibrating partially parallel acquisitions; ICWM, internal capsule white matter; IVIM, intravoxal incoherent motion; MD, mean diffusivity; MK, mean kurtosis; PDF, probability distribution function; PU, putamen; SNR, signal-to-noise ratio; TH, thalamus; WM, white matter.*

Copyright © 2010 John Wiley & Sons, Ltd.

NMR IN BIOMEDICINE

DEFINITIONS

Let $P(\mathbf{r}, t)$ be the water diffusion PDF for a vectorial displacement $\mathbf{r}$ over a time interval t (the diffusion time). The average of an arbitrary function $A(\mathbf{r})$ can then be written

$$\langle A(\mathbf{r})\rangle \equiv \int d^3 r P(\mathbf{r}, t) A(\mathbf{r}), \tag{2}$$

with the angle brackets being introduced as a shorthand for averaging over the PDF. The diffusion coefficient in a direction $\mathbf{n}$ is then defined by

$$D(\mathbf{n}) \equiv \frac{1}{2t}\left\langle (\mathbf{r}\cdot\mathbf{n})^2 \right\rangle, \tag{3}$$

where we assume that $|\mathbf{n}| = 1$. The diffusion coefficient therefore quantifies the variance of the PDF in a given direction. The diffusional kurtosis in the direction $\mathbf{n}$ is similarly defined by

$$K(\mathbf{n}) \equiv \frac{\left\langle (\mathbf{r}\cdot\mathbf{n})^4 \right\rangle}{\left\langle (\mathbf{r}\cdot\mathbf{n})^2 \right\rangle^2} - 3. \tag{4}$$

Eqn (4) is a direct application of the general formula for kurtosis of eqn (1) to molecular diffusion.

The MD corresponds to the average of the diffusion coefficient over all directions, which may be formally expressed as the surface integral

$$\overline{D} \equiv \frac{1}{4\pi}\int d\Omega_{\mathbf{n}} D(\mathbf{n}), \tag{5}$$

with $d\Omega_{\mathbf{n}}$ representing a solid angle element for the direction $\mathbf{n}$. The mean kurtosis (MK) has the analogous definition

$$\overline{K} \equiv \frac{1}{4\pi}\int d\Omega_{\mathbf{n}} K(\mathbf{n}) \tag{6}$$

and is a metric of primary interest for DKI.

In order to quantify diffusional anisotropy, it is useful to define the diffusion tensor

$$D_{ij} \equiv \frac{1}{2t}\langle r_i r_j\rangle \tag{7}$$

and the kurtosis tensor

$$W_{ijkl} \equiv \frac{9}{\langle \mathbf{r}\cdot\mathbf{r}\rangle^2}\left(\langle r_i r_j r_k r_l\rangle - \langle r_i r_j\rangle\langle r_k r_l\rangle - \langle r_i r_k\rangle\langle r_j r_l\rangle - \langle r_i r_l\rangle\langle r_j r_k\rangle\right), \tag{8}$$

where r_i, $i = 1, 2,$ or 3, is a component of the displacement vector $\mathbf{r}$. Both of these tensors are symmetric with respect to interchange of their indices. The diffusion tensor has $3^2 = 9$ components, but because of symmetry only six are independent. The kurtosis tensor has $3^4 = 81$ components, but because of symmetry only 15 are independent. With these two tensors, the diffusion coefficient and diffusional kurtosis in an arbitrary direction can be calculated from

$$D(\mathbf{n}) = \sum_{i,j=1}^{3} n_i n_j D_{ij}, \tag{9}$$

and

$$K(\mathbf{n}) = \frac{\overline{D}^2}{[D(\mathbf{n})]^2}\sum_{i,j,k,l=1}^{3} n_i n_j n_k n_l W_{ijkl}. \tag{10}$$

As a consequence, the full angular variation for the diffusion coefficient is fixed by the 6 independent degrees of freedom for the diffusion tensor, and the full angular variation for the diffusional kurtosis is fixed by the $6 + 15 = 21$ combined degrees of freedom for the diffusion and kurtosis tensors.

It is natural to consider a frame of reference that diagonalizes the diffusion tensor. The direction parallel to the diffusion eigenvector corresponding to the largest diffusion eigenvalue is often referred to as the parallel direction, since in white matter this direction would typically be aligned with axons. One can then define the parallel diffusivity and parallel kurtosis by (11)

$$D_{||} \equiv D(\mathbf{n}_{||}), \tag{11}$$

and

$$K_{||} \equiv K(\mathbf{n}_{||}), \tag{12}$$

where $\mathbf{n}_{||}$ is a unit vector oriented in the parallel direction. One may also define the perpendicular diffusivity and perpendicular kurtosis by

$$D_{\perp} \equiv \frac{1}{2\pi}\int d\Omega_{\mathbf{n}} D(\mathbf{n})\delta(\mathbf{n}\cdot\mathbf{n}_{||}), \tag{13}$$

and

$$K_{\perp} \equiv \frac{1}{2\pi}\int d\Omega_{\mathbf{n}} K(\mathbf{n})\delta(\mathbf{n}\cdot\mathbf{n}_{||}), \tag{14}$$

with $\delta(x)$ indicating the Dirac delta function. For isotropic diffusion, $D_{||} = D_{\perp} = \overline{D}$ and $K_{||} = K_{\perp} = \overline{K}$. An alternative, non-equivalent (but qualitatively similar) definition for $K_{\perp}$ has been proposed by Hui and coworkers (11).

Lätt and coworkers (12) have also considered a kurtosis for the Fourier transform of the PDF. While this Fourier space (q-space) kurtosis also vanishes for Gaussian diffusion, since the Fourier transform of a Gaussian is itself a Gaussian, it is otherwise physically distinct from the diffusional kurtosis as defined by eqn (4).

SIMPLE MODELS

Both the diffusion coefficient and the diffusional kurtosis are model independent diffusion metrics. This is an important advantage, in that it makes them physically well-defined. However, as a consequence of not being tied to a specific tissue model, their interpretation in terms of tissue structure is not always straightforward. For example, the precise mechanism for the diffusion coefficient changes associated with cerebral ischemia in brain has been extensively debated (13–15).

In order to better understand the physical meaning of the diffusional kurtosis, it is helpful to consider idealized diffusion models. Here we consider three basic types: multiple compartment models without water exchange, a two-compartment model with water exchange, and a one-dimensional model with equally spaced semi-permeable barriers. Multiple compartment models are the simplest and most widely applied models for water diffusion in brain, with the compartments representing, for example, intracellualler spaces, extracellular spaces, distinct white matter tracts, and/or cerebrospinal fluid (CSF). The other two types of models are utilized to better understand the effects of water transport between compartments and of diffusion barriers (e.g. cell membranes and organelles), which are not explicitly included in elementary multiple compartment models.

 Copyright © 2010 John Wiley & Sons, Ltd. View this article online at wileyonlinelibrary.com

Multiple compartment models

For a single compartment with Gaussian diffusion, the PDF is given by

$$P(r,t) = \frac{1}{(4\pi t)^{3/2}|\mathbf{D}|^{1/2}} \cdot \exp\left(-\mathbf{r}^T \cdot \mathbf{D}^{-1} \cdot \mathbf{r}/4t\right), \qquad (15)$$

where $\mathbf{D}$ represents the diffusion tensor. One may verify that eqn (15) is consistent with eqn (9) and that it implies $K(\mathbf{n}) = 0$ for all directions. For N Gaussian compartments, eqn (15) is generalized to

$$P(r,t) = \sum_{m=1}^{N} f_m \frac{1}{(4\pi t)^{3/2}\left|\mathbf{D}^{(m)}\right|^{1/2}} \cdot \exp\left\{-\mathbf{r}^T \cdot \left[\mathbf{D}^{(m)}\right]^{-1} \cdot \mathbf{r}/4t\right\}, \qquad (16)$$

where $\mathbf{D}^{(m)}$ is the diffusion tensor for the mth compartment and f_m is the corresponding water fraction. The water fractions are normalized so that

$$1 = \sum_{m=1}^{N} f_m. \qquad (17)$$

From eqns (9) and (16), one finds

$$D(\mathbf{n}) = \sum_{m=1}^{N} f_m D^{(m)}(\mathbf{n}), \qquad (18)$$

with

$$D^{(m)}(\mathbf{n}) \equiv \mathbf{n}^T \mathbf{D}^{(m)} \mathbf{n} \qquad (19)$$

being the diffusion coefficient for the mth compartment in the direction $\mathbf{n}$. Thus the total diffusion coefficient is the weighted sum of the compartmental diffusion coefficients. For the diffusional kurtosis, eqns (9), (10), and (16) lead to (4)

$$K(\mathbf{n}) = 3\frac{\delta^2 D(\mathbf{n})}{[D(\mathbf{n})]^2}, \qquad (20)$$

where $\delta^2 D(\mathbf{n})$ is the diffusion coefficient variance defined by

$$\delta^2 D(\mathbf{n}) \equiv \sum_{m=1}^{N} f_m \left\{\left[D^{(m)}(\mathbf{n}) - D(\mathbf{n})\right]^2\right\}. \qquad (21)$$

The diffusional kurtosis is then simply three times the square of the coefficient of variation for the distribution of compartmental diffusion coefficients. So qualitatively, *the kurtosis is a measure of the heterogeneity of the diffusion environment*. Note also that eqn (20) shows that $K \geq 0$ for any multiple compartment model.

Since two-compartment models have been frequently used to study water diffusion in brain, it is of interest to examine this special case in greater detail. Let $D_1 \equiv D^{(1)}(\mathbf{n})$, $D_2 \equiv D^{(2)}(\mathbf{n})$, and $f \equiv f_1$. Assume further that $D_1 \geq D_2$, so that the $m = 1$ compartment corresponds to the fast diffusing component. Eqns (18) and (20) then reduce to

$$D(\mathbf{n}) = fD_1 + (1-f)D_2, \qquad (22)$$

and

$$K(\mathbf{n}) = 3f(1-f)\frac{(D_1 - D_2)^2}{[D(\mathbf{n})]^2}. \qquad (23)$$

Solving eqns (22) and (23) in terms of D_1 and D_2 yields

$$D_1 = D(\mathbf{n})\left[1 + \sqrt{\frac{K(\mathbf{n})(1-f)}{3f}}\right] \qquad (24)$$

and

$$D_2 = D(\mathbf{n})\left[1 - \sqrt{\frac{K(\mathbf{n})f}{3(1-f)}}\right]. \qquad (25)$$

The physical condition $D_2 \geq 0$ then implies that

$$f \leq \frac{3}{3 + K(\mathbf{n})} \equiv f_b. \qquad (26)$$

Hence knowledge of the kurtosis gives an upper bound on the water fraction for the fast diffusing component of a two-compartment model. The inequality of eqn (26) becomes an equality in the limit $D_1/D_2 \to \infty$. As is suggested by eqn (26), a knowledge of D and K does not uniquely determine the two-compartment model parameters of D_1,D_2, and f.

The parameters D_1,D_2, and f in various brain regions have been estimated by Maier and Mulkern (16) for four normal volunteers. These are reproduced in Table 1 together with values for D, K, and f_b obtained by applying eqns (22), (23), and (26). Note that $K \approx 1$ and that in most regions f_b exceeds f by no more than 20 to 30%.

Kärger model

The multiple compartment models discussed above do not allow for water exchange between compartments. A two-compartment model with water exchange has been proposed by Kärger (17–19) and is often referred to as the Kärger model. The

Table 1. Parameters for two-compartment model obtained from four normal volunteers

Region	D_1 (μm^2/ms)	D_2 (μm^2/ms)	f	D (μm^2/ms)	K	f_b
GM/CSF	1.479 ± 0.166	0.466 ± 0.017	0.490 ± 0.012	0.962 ± 0.083	0.831 ± 0.140	0.783 ± 0.029
GM/WM	1.142 ± 0.106	0.338 ± 0.027	0.622 ± 0.038	0.838 ± 0.073	0.649 ± 0.117	0.822 ± 0.026
TH	1.320 ± 0.164	0.271 ± 0.040	0.617 ± 0.069	0.918 ± 0.125	0.925 ± 0.248	0.764 ± 0.048
PU/GP	1.069 ± 0.039	0.257 ± 0.026	0.648 ± 0.028	0.783 ± 0.035	0.736 ± 0.097	0.803 ± 0.021
FWM	1.155 ± 0.046	0.125 ± 0.014	0.699 ± 0.050	0.845 ± 0.061	0.938 ± 0.206	0.762 ± 0.040
ICWM	1.215 ± 0.024	0.183 ± 0.009	0.637 ± 0.020	0.840 ± 0.026	1.046 ± 0.081	0.741 ± 0.015

Values for D_1, D_2, and f were taken from Ref. 16. Values for D, K, and f_b were calculated using eqns (22), (23), and (26). FWM, frontal white matter; GM/CSF, gray matter next to cerebrospinal fluid; GM/WM, gray matter next to white matter; ICWM, internal capsule white matter; PU/GP, putamen and globus pallidus; TH, thalamus.

View this article online at wileyonlinelibrary.com Copyright © 2010 John Wiley & Sons, Ltd.

NMR IN BIOMEDICINE

independent model parameters are those for the previously discussed two-compartment model (D_1,D_2, and f) plus a residence time, τ_1, for the fast diffusing compartment. The residence time for the slow diffusing compartment is given by $\tau_2 = (1-f)\tau_1/f$, and an exchange time can be defined by $\tau \equiv (1-f)\tau_1 = f\tau_2$. While highly simplified, the Kärger model yields reasonable results for cell suspensions (20) and has been applied to the study of water diffusion in brain (21).

The diffusion coefficient for the Kärger model is given by eqn (22), as for the case without exchange, and is therefore completely independent of the diffusion time. The diffusional kurtosis, in contrast, is given by (4,22)

$$K(t) = K_0 \frac{2\tau}{t}\left[1 - \frac{\tau}{t}\left(1 - e^{-t/\tau}\right)\right], \qquad (27)$$

with $K_0 = K(0)$ being equal to the kurtosis value of eqn (23). As a consequence, *the kurtosis decreases with diffusion time on a scale set by the exchange time*. Figure 1 shows a plot of $K(t)/K_0$ as a function of the ratio t/τ. In order to emphasize the distinct time dependencies of D and K, also plotted in Figure 1 is the trivial line for $D/D_0 = 1$, where D_0 is the initial diffusion coefficient. For very long diffusion times, the kurtosis approaches zero, in consistency with a Gaussian PDF.

The Kärger model thus represents a clear example where the diffusion coefficient and diffusional kurtosis have sharply different behaviors. It also suggests that the kurtosis could be more sensitive to water exchange effects in brain than the diffusion coefficient, although there is as yet no direct empirical evidence for this.

One-dimensional model with barriers

The PDF for one-dimensional diffusion with equally spaced semi-permeable membranes can be determined analytically (23–25). Such a model is of interest because semi-permeable membranes are a primary source of diffusion restrictions in brain as well as other biological tissues. The parameters for the model are the free diffusion coefficient D_f, the spacing between membranes L, and the membrane permeability κ.

For short diffusion times, this model leads to

$$D(t) = D_f\left[1 - \frac{8}{3L}\sqrt{\frac{D_f t}{\pi}} + O(t)\right], \qquad (28)$$

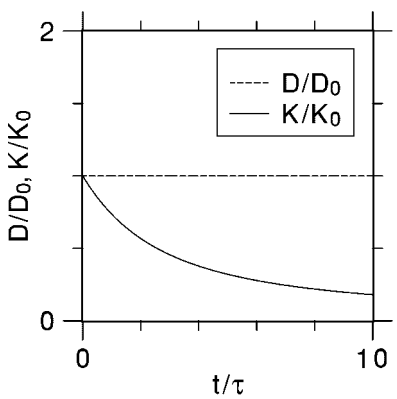

Figure 1. Time dependence of the diffusion coefficient and diffusional kurtosis for the Kärger model. The diffusion coefficient is independent of the diffusion time, but the kurtosis decreases on a time scale set by the water exchange time τ.

and

$$K(t) = \frac{16}{5L}\sqrt{\frac{D_f t}{\pi}} + O(t). \qquad (29)$$

Eqn (28) was derived directly from the one-dimensional diffusion PDF by Sukstanskii and coworkers (25) and is a special case of a more general short time formula for diffusion in restricted media (26,27). The short time expression of eqn (29) for the kurtosis is also a special case of a general result (28). The growth of the kurtosis with diffusion time can be viewed as resulting from an increased diffusional heterogeneity caused by the restriction of water molecules that are initially closest to membranes. The permeability κ does not affect the short time behaviors for either D or K, but does enter into the $O(t)$ corrections.

In the limit of long diffusion times, one may show that,

$$D(t) \approx \frac{\kappa L D_f}{\kappa L + D_f} + \frac{L^2 D_f^2}{12(\kappa L + D_f)^2}\cdot\frac{1}{t}, \qquad (30)$$

and for $\kappa > 0$,

$$K(t) \approx \frac{L D_f}{2\kappa(\kappa L + D_f)}\cdot\frac{1}{t}. \qquad (31)$$

The first term on the right side of eqn (30) corresponds to the famous result of Crick (29), and the second term is also given in the review by Yablonskiy and Sukstanskii of this journal issue. Both the diffusion coefficient and the kurtosis decrease with increasing diffusion time, but the kurtosis approaches zero while the diffusion coefficient approaches a constant. This vanishing of the long time kurtosis is, as for the Kärger model, an indicator that the diffusion PDF becomes Gaussian in this limit. The short time growth and long time reduction for the kurtosis, implied by eqns (29) and (31), show that the kurtosis has a maximum for some intermediate value of the diffusion time.

RELATIONSHIP TO NMR SIGNAL

So far we have discussed the diffusional kurtosis without reference to its measurement with diffusion-weighted NMR/MRI, and it is important to appreciate that the diffusional kurtosis is a well-defined quantity independent of any specific measurement procedure or model. However, the method of estimation for any physical quantity is central to its applications, and in this section, we discuss the relationship between the diffusional kurtosis and the diffusion-weighted NMR signal. For the diffusion-weighted signal, we shall have in mind that obtained for water with the canonical Stejskal-Tanner sequence (1,30), although the essential considerations can be readily extended for many of the other related sequences.

Q-space approach

The most conceptually straightforward approach for measuring the diffusional kurtosis is to first use the NMR signal to calculate the PDF and then determine the kurtosis from eqn (4). The PDF may be calculated from the NMR signal by using established q-space imaging methods (1,30–32), and these have been explicitly applied to the calculation of the kurtosis in brain by some researchers (12,32,33). However for human imaging, q-space methods can be demanding both in terms of hardware requirements and imaging time. In particular, q-space imaging methods typically utilize large maximum b-values of several

 Copyright © 2010 John Wiley & Sons, Ltd. View this article online at wileyonlinelibrary.com

thousand s/mm^2 or more. Therefore, they are often difficult to incorporate into clinical imaging protocols.

Series expansion

DKI attempts to build upon the widespread application and success of DTI by extending the familiar DTI approach to the calculation of the diffusional kurtosis and related diffusion metrics. To see how this is done, let us first review some of the basic principles of DTI. The diffusion-weighted signal intensity, S, can be regarded as a function of the 'b-value,' which for a Stejskal-Tanner sequence is defined by $b \equiv (\gamma\delta g)^2(\Delta - \delta/3)$ where γ is the proton gyromagnetic ratio, g is the amplitude of the diffusion sensitizing magnetic field gradient pulses, δ is the duration of the gradient pulses, and Δ is the time interval between the centers of the gradient pulses (1,30). One can then consider the Taylor series (23,34)

$$\ln[S(b)] = \ln(S_0) - bD_{app} + O(b^2), \quad (32)$$

where D_{app} is the 'apparent' diffusion coefficient and $S_0 \equiv S(0)$. In carrying out the expansion of eqn (32), it is assumed that both Δ and δ are fixed so that b is varied by changing g. In the short pulse duration limit $\delta \to 0$, D_{app} approaches the true diffusion coefficient D for a diffusion time $t = \Delta$. For the special case of multiple, non-exchanging Gaussian compartments, $D_{app} = D$ for arbitrary δ. More generally if we assume the dependence on δ is small, we have the approximation

$$\ln[S(b)] \approx \ln(S_0) - bD(t), \quad (33)$$

for b-values that are sufficiently small so that the $O(b^2)$ terms of eqn (32) are negligible. Here the precise meaning of 'sufficiently small' depends on the sample being studied. The validity of eqn (33) also requires the assumption homogeneous T_2 relaxation within the region of interest (e.g. a voxel). For Gaussian diffusion, eqn (33) is exact, and it can be rewritten in the familiar form

$$S(b) = S_0 e^{-bD}. \quad (34)$$

By fitting eqn (33) to signal intensity data for a range of b-values, an estimate for D may be obtained. These data should all be for the same gradient direction, which then determines the diffusion direction for D. For any single direction, at least two b-values are needed, since eqn (33) has two unknowns. If exactly two b-values, b_1 and b_2, are used, we then have the closed-form solution

$$D \approx \frac{1}{b_2 - b_1} \cdot \ln\left[\frac{S(b_1)}{S(b_2)}\right]. \quad (35)$$

Of course, in applying eqns (33) or (35), it is important to choose the range of b-values appropriately. If the maximum b-value is too low, then the variation of the signal intensity will be small and estimates for D will be extremely sensitive to noise. If the maximum b-value is too high, then there will be systematic errors in measured D values due to the neglecting of the $O(b^2)$ term of in eqn (33). For brain, experience has shown that a maximum b-value of about 1000 s/mm^2 provides a reasonable compromise between precision and accuracy, and this value is now a widely used standard.

DKI is based on similar logic with the key difference being that eqn (32) is replaced with the expression

$$\ln[S(b)] = \ln(S_0) - bD_{app} + \frac{1}{6}b^2D_{app}^2K_{app} + O(b^3), \quad (36)$$

which now explicitly includes the $O(b^2)$ term (3,4). Eqn (36) corresponds to a cumulant expansion for the diffusion NMR signal, as has been discussed in several prior studies (23,34–36). Here K_{app} is the apparent diffusional kurtosis, which approaches the true kurtosis K in the limit of short pulse durations. Also, for multiple, non-exchanging Gaussian compartment models, $K_{app} = K$ for arbitrary δ, in analogy with the diffusion coefficient. The DKI extension of eqn (33) is then

$$\ln[S(b)] \approx \ln(S_0) - bD(t) + \frac{1}{6}[bD(t)]^2K(t), \quad (37)$$

for b-values that are sufficiently small so that the $O(b^3)$ terms of eqn (36) are negligible. As for DTI, the meaning of 'sufficiently small' is, in general, sample dependent, but will typically include a larger range of b-values than for eqn (33) due to the inclusion of the higher order term. With this approximation, one can estimate both D and K by fitting to diffusion-weighted signal intensity data with three or more b-values (since there are now 3 unknowns) in any given gradient direction. For exactly three b-values, b_1, b_2 and b_3, the closed-form expressions are [37]

$$D \approx \frac{(b_3 + b_1)D^{(12)} - (b_2 + b_1)D^{(13)}}{b_3 - b_2}, \quad (38)$$

and

$$K \approx 6\frac{D^{(12)} - D^{(13)}}{(b_3 - b_2)D^2}, \quad (39)$$

where

$$D^{(12)} \equiv \frac{\ln\left[\frac{S(b_1)}{S(b_2)}\right]}{b_2 - b_1}, D^{(13)} \equiv \frac{\ln\left[\frac{S(b_1)}{S(b_3)}\right]}{b_3 - b_1}. \quad (40)$$

Note that $D^{(12)}$ and $D^{(13)}$ correspond to the DTI estimates of the diffusion coefficient for the b-values pairs of (b_1, b_2) and (b_1, b_3), respectively. Figure 2 gives a comparison of the DTI and DKI fits for a simulated data set.

Maximum b-values for DKI

In order to obtain accurate parameter estimates with DKI, it is necessary, as for DTI, to be careful in choosing the maximum

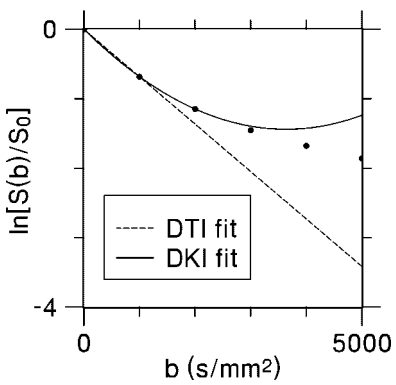

Figure 2. Comparison of DTI and DKI fitting models. For DTI, the logarithm of diffusion-weighted signal intensity (circles) as a function of the b-value is fit, for small b-values, to a straight line. In brain, this fit is often based on the signal for $b = 0$ and $b = 1000$ s/mm^2. For DKI, the logarithm of the signal intensity is fit, for small b-values, to a parabola. In brain, this fit may be based on the signal for $b = 0$, $b = 1000$, and $b = 2000$ s/mm^2.

View this article online at wileyonlinelibrary.com Copyright © 2010 John Wiley & Sons, Ltd.

NMR IN BIOMEDICINE

b-values. These will typically be larger than for DTI, since for DKI we do not want the $O(b^2)$ terms to be negligible.

If we make the assumption that $S(b)$ is a monotonically decreasing function of the b-value, then one can derive the upper bound of (38)

$$b \leq \frac{3}{DK} \tag{41}$$

as a necessary condition for the validity of eqn (37). This assumption of a monotonically decreasing signal intensity is empirically true for brain and most other biological tissues, but it can fail to hold for certain specially structured media (39). As Table 1 indicates, typical values in brain are roughly $D \approx 1\mu m^2/ms$ and $K \approx 1$. These then imply the upper bound of $b \leq 3000\,s/mm^2$.

While eqn (41) is quite general and a useful guide, it is not sufficient to guarantee that eqn (37) will yield accurate estimates for D and K. To more precisely determine a suitable b-value range, we exploit the observation that signal intensity data in brain are well approximated with biexponential curves up to b-values of about $5000\,s/mm^2$ (16). Thus as a representative model, it is reasonable to take

$$S(b)/S_0 = fe^{-bD_1} + (1-f)e^{-bD_2}. \tag{42}$$

This is precisely the signal decay form for a non-exchanging, two-compartment Gaussian diffusion model, which we have already discussed, with one compartment having a diffusion coefficient D_1 and a water fraction f and the other compartment having a diffusion coefficient D_2 and a water fraction $1-f$. As before, we may assume without loss of generality that $D_1 \geq D_2$. For this model, the exact values for D and K are given by eqns (22) and (23).

Now let us consider applying eqn (37) to estimate D and K for the signal intensity of eqn (42) with the b-values chosen, for sake of simplicity, to be: $b_1 = 0$, $b_2 = b_{max}/2$, and $b_3 = b_{max}$. Since there are exactly three b-values, we can apply eqns (38) and (39) to find

$$D_{fit} \approx 2D^{(12)} - D^{(13)}, \tag{43}$$

and

$$K_{fit} \approx 12\frac{D^{(12)} - D^{(13)}}{D_{fit}^2 b_{max}}, \tag{44}$$

where we have added a subscript 'fit' to indicate that these estimates are based on a fit for the series approximation of eqn (37). These 'fit' values may then be compared to the exact values from eqns (22) and (23) in order to assess the accuracy obtained by the use of eqn (37).

In Figure 3a, the ratio K_{fit}/K, with K being the exact kurtosis, is plotted for $K = 1$, $0 \leq f \leq f_b$, and $Db_{max} = 1$, 2, and 3. For given values of D, K, and f, D_1 was calculated from eqn (24), D_2 was calculated from eqn (25), and f_b was calculated to be 3/4 from eqn (26). We have made the choice of $K = 1$, since this is a typical value for brain. The curve for $Db_{max} = 3$ corresponds, for $K = 1$, to the bound of eqn (41). At this upper limit, the K_{fit} values are accurate to within about 20% for $0.6 \leq f \leq f_b$. For $Db_{max} = 2$, this 20% accuracy interval grows to $0.52 \leq f \leq f_b$, which covers the range for most brain regions with a bit of a margin (see Table 1). A similar plot for D_{fit}/D is shown in Figure 3b. For $Db_{max} = 3$, the accuracy is about 10% or better for the full range of f values, while for $Db_{max} = 2$, the accuracy is better than 7%. As a comparison, Figure 3c shows the corresponding plot for D_{DTI}/D, where D_{DTI} is calculated from the usual DTI formula of eqn (35) with $b_1 = 0$ and $b_2 = b_{max}$. The DTI approximation is accurate to within about 20% for $Db_{max} = 1$.

Since $D \approx 1\mu m^2/ms$ in brain, DKI with $b_{max} = 2000\,s/mm^2$ should, based on this calculation, yield estimates for the diffusional kurtosis with an accuracy of roughly 20% or better and for the diffusion coefficient with an accuracy of roughly 7% or better. This is comparable to the 20% accuracy found for the DTI-based diffusion coefficient estimates with $b_{max} = 1000\,s/mm^2$. The accuracy of K_{fit} is, however, more strongly dependent on f than for either D_{fit} or D_{DTI}. These conclusions are, of course, all dependent on the correctness of our assumption that biexponential signal decay is a reasonable approximation for brain.

That the series approximation of eqn (37) is fairly accurate for brain up to b-values of 2000 to $3000\,s/mm^2$ is consistent with prior studies that have directly studied fits to brain signal intensity data (4,5,40). Most prior DKI brain studies (4,5,11, 37,38,41–45) have been confined to this b-value range, although a few have used somewhat larger maximum values (12,46,47).

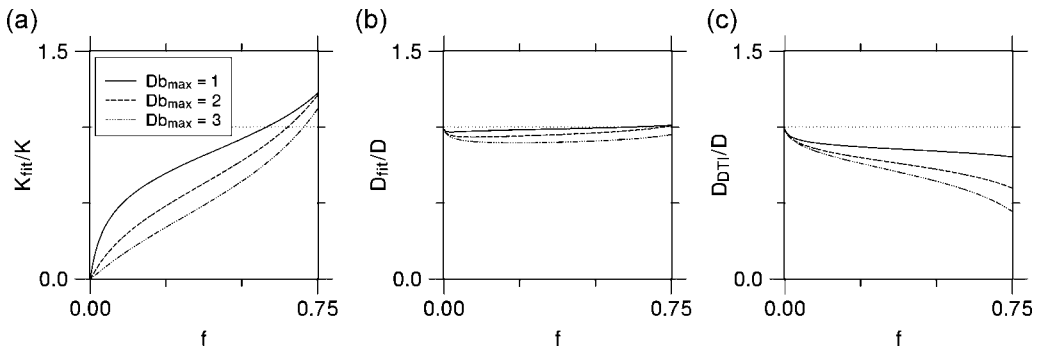

Figure 3. Plots showing the ratio of DKI estimates for (a) the diffusional kurtosis and (b) the diffusion coefficient to the exact values for a two-compartment diffusion model with $K = 1$. For this model, the water fraction f of the fast diffusing component can vary from 0 to 0.75, as follows from eqn (26). The DKI fits are based on eqns (43) and (44). The dotted lines are references to indicate the ideal estimate ratio of one. Plot (a) shows that the DKI estimate for the kurtosis is accurate to within about 20% if $f \geq 0.52$ and $Db_{max} = 2$, and plot (b) shows that the DKI estimate for the diffusion coefficient is accurate to within about 7% if $Db_{max} = 2$. As indicated by Table 1, $f \approx 0.6$ to 0.7 for normal brain, suggesting that DKI with $Db_{max} = 2$ should be reasonably accurate. As a comparison, also shown is (c) the ratio of the DTI estimate for the diffusion coefficient to the exact value for the same two-compartment model. The DTI fit is calculated from eqn (35) with $b_1 = 0$ and $b_2 = b_{max}$. The DTI estimate is accurate to within about 20% if $Db_{max} = 1$.

 Copyright © 2010 John Wiley & Sons, Ltd. View this article online at wileyonlinelibrary.com

In practice, the optimum choice of maximum b-value, for both DTI and DKI, is a compromise between precision and accuracy. The effects of diffusion on the signal intensity increase with increasing b-value, but the accuracies of eqns (33) and (37) decrease. For MRI of the brain, *empirical* evidence indicates that maximum b-values of about 1000 s/mm^2 for DTI and of 2000 to 3000 s/mm^2 for DKI are appropriate. For tissues other than brain, for fixed brain tissue, or for phantoms, it is crucial that an appropriate b-value range be independently established before applying eqn (37). Otherwise, significant errors in parameter estimates may occur (48).

Other signal intensity models

Eqn (36) demonstrates that the diffusional kurtosis is determined by the small b-value behavior of $S(b)$. It is for this reason that a full q-space imaging approach is not necessary to estimate the kurtosis, which allows for the acquisition of a reduced data set and for a simplified analysis method. In addition, eqn (36) suggests the previously discussed fitting model based on eqn (37), which is usually employed as a part of DKI. However, eqn (36) can also be applied to other $S(b)$ models, which may at times offer some advantages over eqn (37).

The key requirement is that the model for $S(b)$ be analytic in the b-value about $b = 0$. The model parameters can be related to the kurtosis by carrying out a Taylor series for $\ln[S(b)]$ and comparing the coefficients for the $O(b)$ and $O(b^2)$ terms with eqn (36). For example, applying this procedure to the biexponential signal decay of eqn (42) leads directly to the expressions of eqns (22) and (23).

Besides the two-compartment (biexponential) model, other proposed models for $S(b)$ in brain include a statistical model of Yablonskiy and coworkers (49), a random cylinder model of Jespersen and coworkers (50), and Pearson distribution models of Poot and coworkers (51). Such models may be of interest either because they are motivated by a microscopic model of water diffusion in brain (49,50) or because they have desirable numerical properties (51).

As a simple further illustration, consider the statistical model based on a gamma distribution of diffusion coefficients. This corresponds to a multiple compartment model where the water fraction density for a compartment with diffusion coefficient D' is given by

$$F(D') = \frac{\beta^\alpha}{\Gamma(\alpha)}(D')^{\alpha-1}\exp(-\beta D'), \qquad (45)$$

with $\Gamma(\alpha)$ being Euler's gamma function. The parameters α and β set the mean (α/β) and variance (α/β^2) of the gamma distribution, and normalizability requires that both α and β be positive. A closely related model has been previously discussed by Jian and coworkers (52). If the individual compartments are assumed to have Gaussian diffusion, the total signal intensity is then

$$S(b)/S_0 = \int_0^\infty dD' F(D')\exp(-bD') = \frac{\beta^\alpha}{(\beta+b)^\alpha}. \qquad (46)$$

Expanding eqn (46) in powers of the b-value and comparing with eqn (36) leads to the identifications $\alpha = 3/K$ and $\beta = 3/KD$. The signal intensity for this model then takes on the form

$$S(b)/S_0 = \left(1 + \frac{KDb}{3}\right)^{-3/K}. \qquad (47)$$

The requirement $\alpha > 0$ means that the kurtosis must also be positive for this model. The Taylor expansion for $\ln[S(b)]$ is

$$\ln[S(b)] = \ln(S_0) - bD + \frac{1}{6}b^2D^2K - \frac{1}{27}b^3D^3K^2 + O(b^4). \qquad (48)$$

Thus if $b << 27/(6DK)$, then the $O(b^3)$ term is dominated by the lower order terms and fits for the model of eqn (47) will give similar results for the kurtosis as fits for the model of eqn (37). It is also interesting to note that the radius of convergence for the expansion of eqn (48) is $3/DK$, which is exactly the upper bound of eqn (41).

So for sufficiently small b-values, models such as that of eqn (47) will be effectively equivalent to the standard DKI fitting form of eqn (37), and eqn (37) may be preferable in practice because of its simplicity and because it allows one to avoid nonlinear fitting procedures (37). However, for larger b-values, alternative models may well provide a better description of the signal intensity data, and they may be convenient and useful if high b-value data are acquired.

A comparison of exemplary Gaussian, two-compartment, and gamma distribution diffusion models is given in Figure 4. For all three models, the parameters have been chosen so that $D = 1\mu m^2/ms$. For the Gaussian model $K = 0$, while for both the two-compartment and gamma distribution models $K = 1$. The water fraction for the fast diffusing component of the two-compartment model is $f = 2/3$, which is similar to the values for brain listed in Table 1. The water fraction densities $F(D')$ for all three models are given in Figure 4a, and the corresponding signal intensities and PDFs are given in Figures 4b and 4c. Also shown in Figure 4b is the DKI signal intensity of eqn (37) for $D = 1\mu m^2/ms$ and $K = 1$. The DKI signal intensity matches within 20% that for the two-compartment model up to a b-value of about 3400 s/mm^2 and that for the gamma distribution model up to a b-value of about 2000 s/mm^2. The PDFs of Figure 4c are for a diffusion time of t=100 ms and assume isotropic diffusion. Note that these are three-dimensional PDFs with dimensions of inverse volume cubed, rather than one-dimensional PDFs for a particular diffusion direction. The PDF for the Gaussian model was calculated from eqn (15), the PDF for the two-compartment model was calculated from eqn (16) with $N = 2$, and the PDF for the gamma distribution model was calculated by applying standard q-space imaging techniques (31) to the signal decay form of eqn (47).

One model that is inconsistent with DKI is the stretched-exponential, which has also been applied to describe diffusion-weighted signal intensity data and uses the form

$$S(b)/S_0 = \exp[-(b \cdot DDC)^\alpha], \qquad (49)$$

where DDC represents a 'distributed diffusion coefficient' (53). For non-integer values of α, $\ln[S(b)]$ has a singularity at $b = 0$ and the expansion of eqn (36) is not possible. So for this model, neither the diffusion coefficient nor the diffusional kurtosis is well-defined.

DATA ACQUISITION

In order to fully characterize the directional dependence in anisotropic tissues, such as white matter, for both the diffusion

View this article online at wileyonlinelibrary.com Copyright © 2010 John Wiley & Sons, Ltd.

NMR IN BIOMEDICINE

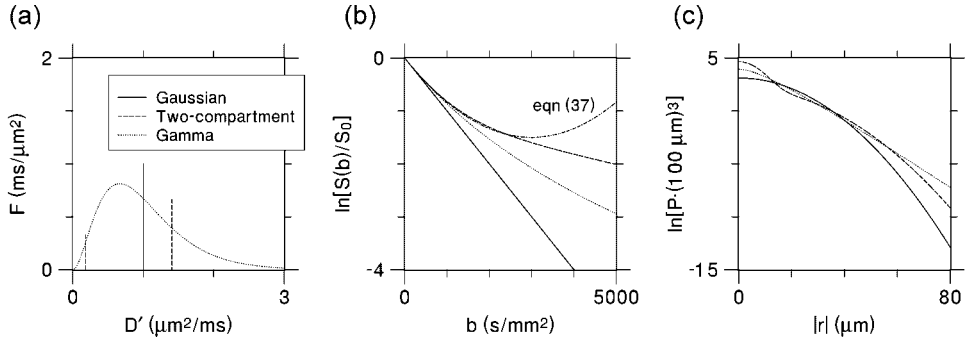

Figure 4. Plots showing (a) the water fraction densities for Gaussian, two-compartment, and gamma distribution diffusion models together with the logarithms of the corresponding (b) signal intensities and (c) PDFs. In (a), the vertical lines for the Gaussian and two-compartment models indicate Dirac delta functions with weights proportional to the heights of the lines. For the two-compartment model, the water fraction for the fast diffusing component is $f = 2/3$. All three models have a diffusion coefficient of $D = 1\mu m^2/ms$, while the Gaussian model has a diffusional kurtosis of $K = 0$ and the two-compartment and gamma distribution models both have $K = 1$. Also shown in (b) is the DKI signal intensity of eqn (37) for $D = 1\mu m^2/ms$ and $K = 1$, which agrees relatively well with both the two-compartment and gamma distribution models up to $b \approx 2000\,s/mm^2$ and with the two-compartment model up to $b \approx 3400\,s/mm^2$. The PDFs in (c) assume isotropic diffusion with a diffusion time of $t = 100\,ms$, which yields a root-mean-square diffusion length of $\sqrt{6Dt} \approx 24\mu m$. The PDFs have been normalized by multiplying with a volume element of $(100\,\mu m)^3$. The PDFs for the two-compartment and gamma distribution models both deviate significantly from the Gaussian PDF, as is reflected by their nonzero kurtoses.

coefficient and the diffusional kurtosis, one must determine the diffusion and kurtosis tensors. Since the diffusion tensor has 6 degrees of freedom and the kurtosis tensor has 15 degrees of freedom, there are a total of 21 parameters to be estimated. This implies that at least 22 diffusion-weighted signal intensity images must be acquired for DKI, as there is also one degree of freedom associated with S_0. It can be further shown that there must be, in general, at least three distinct b-values and at least 15 distinct diffusion (gradient) directions. Consistent with these basic constraints, a wide range of DKI data acquisition protocols are possible. While it is valuable to consider a formal optimization of the choice of b-values and directions (54), here we confine ourselves to recommendations based on our experience with performing DKI on a Siemens Trio 3T MRI scanner using a body coil for transmission and a twelve-element phase array head coil for reception.

Early investigations of DKI utilized 6 b-values ranging from 0 to $2500\,s/mm^2$ in increments of $500\,s/mm^2$ (4,5). An advantage of using more than 3 b-values is that this permits the fitting model's goodness-of-fit to be assessed. However, if the model (i.e. eqn (37)) is considered valid, then we have found it more efficient and convenient to simply use the 3 b-values of 0, 1000, and $2000\,s/mm^2$ (37). This is a minimal extension of the usual DTI choice of $b = 0$ and $1000\,s/mm^2$, and we now consider a 3 b-value protocol to be the standard in our laboratory for DKI of brain.

Although the minimum number of diffusion directions is 15, we typically use 30 directions for two primary reasons. First, oversampling of the diffusion directions makes the final estimates for the DKI metrics less sensitive to motion artifacts, such as those caused by cardiac-induced brain pulsation. Second, by using more directions, one effectively averages over some of the higher angular frequencies associated with the neglected terms of the series expansion of eqn (36) for $\ln[S(b)]$. In addition, 30 directions is a particularly convenient choice, because the diffusion directions can then be chosen to lie on the vertices of a truncated icosahedron (buckyball); this shape is an Archimedean solid with 60 vertices that are all equivalent up to a rotation. Since the diffusion-weighted signal is invariant with respect to a reflection of the diffusion directions through the origin, only half of these vertices need be employed.

With these choices for b-values and directions, we are able to acquire acceptable whole brain DKI data with a vendor supplied diffusion-weighted pulse sequence (software version: VB13; sequence name: ep2d_diff) and the imaging parameters: voxel size $= 3 \times 3 \times 3\,mm^3$, field of view $= 222 \times 222\,mm^2$, acquisition matrix $= 74 \times 74$, number of slices $= 39$, inter-slice gap $= 0$, TE $=$ 96 ms, TR $= 5100$ ms, averages $= 1$, partial Fourier encoding $= 3/4$, parallel imaging acceleration (GRAPPA) factor $= 2$, and $b = 0$ averages $= 10$. The total acquisition time for this protocol is 6 min and 37 s. The data are acquired in two blocks; a main block (acquisition time $= 5$ min 26 s) with 3 b-values and 30 directions and a secondary block (acquisition time $= 1$ min 1 s) with the nine additional $b = 0$ images. The reason for this partitioning is that the diffusion-weighted sequence is designed to give just one $b = 0$ image per average so that this is all that is obtained from the main block. Altogether 10 $b = 0$ images are acquired, which allows for a sufficient amount of signal averaging. The relatively short acquisition time is, in part, a consequence of the 100% duty cycle achievable for this sequence on the Siemens Trio system.

In order to obtain a better resolution, we also utilize a similar protocol, but with $2.7 \times 2.7 \times 2.7\,mm^3$ voxels, acquisition matrix $= 82 \times 82$, 45 slices, TR $= 5900$ ms, and two averages for the main block. The total acquisition time for this variant is 13 min 47 s. The application of partial Fourier encoding in the above DKI protocols is helpful in reducing TE, thereby increasing the effective signal-to-noise ratio (SNR) and reducing the acquisition time. However, one recent study has reported significant artifacts in diffusion-weighted images associated with partial Fourier encoding (55). These were shown to result from motion induced by mechanical vibrations and could be eliminated by using full Fourier encoding. Such artifacts have not been evident with our DKI protocols, but their origin suggests that they may be strongly dependent on both imaging protocol details and the particular mechanical properties of the MRI scanner.

POST-PROCESSING

Just as for DTI, there are a variety of post-processing methods for DKI data. As an example, we describe here one approach based on a 3 b-value data acquisition. It differs from a previously

 Copyright © 2010 John Wiley & Sons, Ltd. View this article online at wileyonlinelibrary.com

proposed method (5) mainly in that it exploits the use of exactly 3 b-values and in that it applies some new analytic formulae for $\overline{K}$, $K_{||}$, and $K_{\perp}$.

Let us assume we have a set of images that, following the usual steps of co-registration, averaging, and (optionally) smoothing, consist of one $b = 0$ image and, for each of N (≥ 15) diffusion directions, two $b > 0$ images. We then calculate for each direction, on a voxel-by-voxel basis, a diffusion coefficient and a diffusional kurtosis by applying eqns (38)(40) with $b_1 = 0$. For the two $b > 0$ b-values, b_2 and b_3, we assume $b_3 > b_2$.

Because of noise, motion, and/or imaging artifacts, it is likely that some fraction of the calculated diffusion coefficients and diffusional kurtoses will lie outside a range considered physically acceptable. We typically require that the diffusion coefficients be positive and that the kurtoses lie between a predefined minimum value, K_{min}, and a predefined maximum value, K_{max}. Any outlier values are systematically brought into this range. For example, if the diffusion coefficient is calculated to be less than zero, then both the diffusion coefficient and the kurtosis are reset to zero. In this manner, the effect of noise, motion, and imaging artifacts on the final diffusion metric maps can be substantially reduced. The parameter K_{min} is always between -2 (the theoretical kurtosis minimum) and 0, with 0 being the standard choice. The parameter K_{max} is set to $C/(b_3 D)$, where $C \geq 3$ and D is the diffusion coefficient for the given direction. The constant C is normally set to a value of 3 in order to be consistent with the condition of eqn (41).

The next step is to calculate the diffusion tensor, for each voxel, using the N calculated diffusion coefficients. This is performed exactly as for DTI by solving a linear system for the tensor components (6). The diffusion tensor and eqn (9) are then applied to determine, for each direction, a recalculated diffusion coefficient, $D_i^{(R)}$, $i = 1, 2, \ldots, N$, with the subscript i indicating the direction. From these, a recalculated diffusional kurtosis is found from

$$K_i^{(R)} = 6\frac{D_i^{(R)} - D_i^{(13)}}{(b_1 + b_3)\left[D_i^{(R)}\right]^2}, \tag{50}$$

so as to be consistent with the recalculated diffusion coefficients. Any of the recalculated diffusion and kurtosis values outside the specified physical range for these parameters are again corrected. This recalculation procedure helps to further suppress the effects of noise.

The kurtosis tensor is then found from the diffusion tensor and the set of N recalculated kurtosis values by the solving a linear system (5). This linear system has N equations, which determine the 15 degrees of freedom for the kurtosis tensor.

In order to calculate the diffusion metrics of most interest, it is convenient to first rotate each voxel's coordinate system so that the diffusion tensor is diagonal, with the eigenvalues $\lambda_1 \geq \lambda_2 \geq \lambda_3$. As is well known (9), the MD and FA are then given by

$$\overline{D} = \frac{1}{3}(\lambda_1 + \lambda_2 + \lambda_3), \tag{51}$$

and

$$FA = \sqrt{\frac{(\lambda_1 - \lambda_2)^2 + (\lambda_1 - \lambda_3)^2 + (\lambda_2 - \lambda_3)^2}{2(\lambda_1^2 + \lambda_2^2 + \lambda_3^2)}}. \tag{52}$$

In addition, the axial and radial diffusivities can be calculated from

$$D_{||} = \lambda_1, \tag{53}$$

and

$$D_{\perp} = \frac{1}{2}(\lambda_2 + \lambda_3). \tag{54}$$

These four DTI metrics are not all independent since $\overline{D} = (D_{||} + 2D_{\perp})/3$.

Similar, albeit more complicated formulae, can also be given for the mean, axial, and radial kurtoses. For the MK, we have

$$\begin{aligned}\overline{K} = {} & F_1(\lambda_1, \lambda_2, \lambda_3)\tilde{W}_{1111} + F_1(\lambda_2, \lambda_1, \lambda_3)\tilde{W}_{2222} \\ & + F_1(\lambda_3, \lambda_2, \lambda_1)\tilde{W}_{3333} + F_2(\lambda_1, \lambda_2, \lambda_3)\tilde{W}_{2233} \\ & + F_2(\lambda_2, \lambda_1, \lambda_3)\tilde{W}_{1133} + F_2(\lambda_3, \lambda_2, \lambda_1)\tilde{W}_{1122},\end{aligned} \tag{55}$$

where $\tilde{W}_{ijkl}$ are components of the kurtosis tensor in the frame of reference that diagonalizes the diffusion tensor,

$$F_1(\lambda_1, \lambda_2, \lambda_3) \equiv \frac{(\lambda_1 + \lambda_2 + \lambda_3)^2}{18(\lambda_1 - \lambda_2)(\lambda_1 - \lambda_3)}\left[\frac{\sqrt{\lambda_2\lambda_3}}{\lambda_1}R_F\left(\frac{\lambda_1}{\lambda_2}, \frac{\lambda_1}{\lambda_3}, 1\right) + \frac{3\lambda_1^2 - \lambda_1\lambda_2 - \lambda_2\lambda_3 - \lambda_1\lambda_3}{3\lambda_1\sqrt{\lambda_2\lambda_3}}R_D\left(\frac{\lambda_1}{\lambda_2}, \frac{\lambda_1}{\lambda_3}, 1\right) - 1\right], \tag{56}$$

and

$$F_2(\lambda_1, \lambda_2, \lambda_3) \equiv \frac{(\lambda_1 + \lambda_2 + \lambda_3)^2}{3(\lambda_2 - \lambda_3)^2}\left[\frac{\lambda_2 + \lambda_3}{\sqrt{\lambda_2\lambda_3}}R_F\left(\frac{\lambda_1}{\lambda_2}, \frac{\lambda_1}{\lambda_3}, 1\right) + \frac{2\lambda_1 - \lambda_2 - \lambda_3}{3\sqrt{\lambda_2\lambda_3}}R_D\left(\frac{\lambda_1}{\lambda_2}, \frac{\lambda_1}{\lambda_3}, 1\right) - 2\right]. \tag{57}$$

In eqns (56) and (57), R_F and R_D represent Carlson's elliptic integrals (56,57). The derivation of eqns (55)–(57) may be accomplished by explicitly performing the surface integral of eqn (6) with the help of eqns (9) and (10). The functions F_1 and F_2 have removable singularities when two or more of the eigenvalues coincide; these should be carefully treated in any numerical implementation.

For the axial kurtosis, the corresponding expression is

$$K_{||} = \frac{(\lambda_1 + \lambda_2 + \lambda_3)^2}{9\lambda_1^2}\tilde{W}_{1111}, \tag{58}$$

and for the radial kurtosis, it is

$$\begin{aligned}K_{\perp} = {} & G_1(\lambda_1, \lambda_2, \lambda_3)\tilde{W}_{2222} + G_1(\lambda_1, \lambda_3, \lambda_2)\tilde{W}_{3333} \\ & + G_2(\lambda_1, \lambda_2, \lambda_3)\tilde{W}_{2233},\end{aligned} \tag{59}$$

where

$$G_1(\lambda_1, \lambda_2, \lambda_3) = \frac{(\lambda_1 + \lambda_2 + \lambda_3)^2}{18\lambda_2(\lambda_2 - \lambda_3)^2}\left(2\lambda_2 + \frac{\lambda_3^2 - 3\lambda_2\lambda_3}{\sqrt{\lambda_2\lambda_3}}\right), \tag{60}$$

and

$$G_2(\lambda_1, \lambda_2, \lambda_3) = \frac{(\lambda_1 + \lambda_2 + \lambda_3)^2}{3(\lambda_2 - \lambda_3)^2}\left(\frac{\lambda_2 + \lambda_3}{\sqrt{\lambda_2\lambda_3}} - 2\right). \tag{61}$$

View this article online at wileyonlinelibrary.com Copyright © 2010 John Wiley & Sons, Ltd.

NMR IN BIOMEDICINE

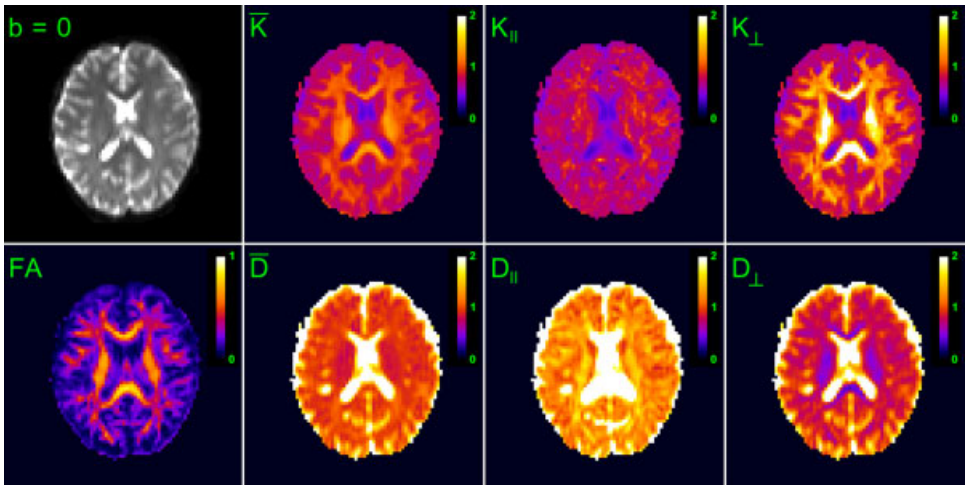

Figure 5. DKI diffusion metric maps for a single axial slice together with a T_2-weighted ($b = 0$) image from one normal subject. The diffusion-weighted data were acquired at 3T with b-values of 0, 1000, and 2000 s/mm^2. The maps for FA, $\overline{D}$, $D_{||}$, and $D_{\perp}$ are similar to those typically obtained with DTI. The maps for $\overline{K}$, $K_{||}$, and $K_{\perp}$ provide additional information that quantify diffusional non-Gaussianity. The calibration bars for the diffusivities are in units of μm^2/ms, while those for the FA and kurtoses are dimensionless.

We emphasize again that this radial kurtosis differs from that defined by Hui and coworkers (11). Note the removable singularities for G_1 and G_2.

By applying the eqns (55)–(61), DKI provides three metrics of diffusional non-Gaussianity, in addition to the diffusion metrics routinely found with DTI. In principle, DKI can provide even more new metrics, since the kurtosis tensor has 15 degrees of freedom. In fact, the components of the kurtosis tensor in the frame of reference that diagonalizes the diffusion tensor can all be regarded as rotational invariants and hence as possible metrics of interest. Alternatively, one may define 'eigenvalues' for the kurtosis tensor, which are also candidates for useful diffusion measures (58–60). However, for isotropic diffusion, such as is a good approximation for gray matter, the only two independent diffusion measures that can be obtained with DKI are the MD and the MK.

Sample parametric maps obtained with the above procedure are shown in Figure 5. The diffusion-weighted imaging data for these maps were obtained on a Siemens 3T scanner using the protocol described under Data Acquisition with $2.7 \times 2.7 \times 2.7$ mm^3 voxels and two averages. The subject gave informed consent and the protocol was approved by the New York University School Medicine Institutional Review Board. Post-processing used $K_{\min} = 0$ and $C = 3$. In Figure 6, the corresponding whole brain parametric distribution plots are shown. Voxels with MD values above 1.5 μm^2/ms were excluded since they were presumed to contain substantial amounts of CSF. The distribution plot for the MK appears bimodal, reflecting the different kurtoses for gray and white matter. The average MD and MK values of Figure 6 are similar to the ones listed in Table 1, even though they were derived using different signal intensity models.

CONFOUNDING FACTORS

It is important to bear in mind that there are a number factors that can lead to errors in diffusional kurtosis values as estimated with DKI, which are essentially the same those that can lead to errors for DTI (61). These include inhomogeneous T_2 relaxation, gradient pulse duration effects, motion, imaging artifacts, perfusion, CSF contamination, inaccuracy of fitting model, not fully accounting for imaging gradient contributions to b-values, and noise, and the influence of these factors may depend on the diffusion time. So the moniker 'apparent' is well-deserved for both MRI-estimated diffusion coefficients and diffusional kurtoses. Although the accuracy of DTI or DKI parameter estimates

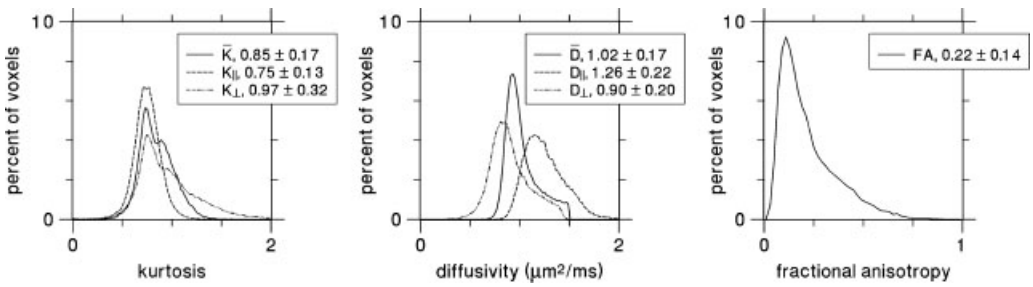

Figure 6. Whole brain distribution plots for DKI diffusion metrics for the same subject as in Fig. 5. The distributions were calculated from 45 axial slices each with a thickness of 2.7 mm. Voxels with $\overline{D} > 1.5$ μm^2/ms were excluded, as they likely contained high amounts of CSF. Each plot was based on 53,881 voxels, corresponding to a total volume of 1060.5 cm^3, and a bin size of 0.02 (in units of μm^2/ms for the diffusivities). The values in the legends indicate average values ± standard deviations.

 Copyright © 2010 John Wiley & Sons, Ltd. View this article online at wileyonlinelibrary.com

may be modest, the precision can be relatively high for carefully performed experiments. The reproducibility the DKI measures of non-Gaussianity is similar to that for standard DTI metrics.

For DKI, noise is particularly important due to the use of higher maximum b-values than for DTI, and an inadequate SNR tends to cause overestimation of kurtosis values. At 3T, the globus pallidus provides a useful test of the SNR. If the SNR is adequate, its MK value in normal brain should be similar to that of other gray matter regions (see Table 1). However with a low SNR, the globus pallidus MK can become relatively elevated because the SNR effect is enhanced by the comparatively short T_2 for the globus pallidus. Noise correction procedures that have been developed for diffusion-weighted imaging (62) should be beneficial for DKI, although this has yet to be systematically explored.

Perfusion affects diffusion-weighted imaging through the intravoxal incoherent motion (IVIM) mechanism (63). The IVIM effect is usually small in normal brain, due to low blood volume and a short T_2 for venous blood, but this is potentially not the case for some brain tumors with high blood volumes. IVIM alters the diffusion-weighted signal intensity primarily for b-values in the range of 0 to 300 s/mm^2 (64,65), and diffusion-weighted data for this range should be examined when applying DKI to tumors. If IVIM effects are substantial for low b-values, then a DKI analysis could be applied with a minimum b-value set to approximately 300 s/mm^2 in order to reduce the influence of perfusion on estimates for DKI diffusion metrics.

APPLICATIONS

DTI is a mature imaging technique with several established brain applications, including ischemic stroke, brain tumors and fiber tracking (66–69). DKI, on the other hand, is still in an early stage of development, and its practical utility remains to be proven. However, since DKI is an extension of DTI and enables the calculation all the usual DTI metrics, it is natural to speculate that DKI will be useful for many of the same applications as DTI. The potential advantage of DKI over DTI is that the added metrics quantifying diffusional non-Gaussianity may supply new information to better characterize both normal and pathological brain tissue. This may be particularly important in gray matter, since gray matter diffusion is nearly isotropic which limits the value of the FA and other metrics of diffusional anisotropy obtainable with DTI.

Diffusional kurtosis metrics may complement diffusion coefficient metrics in at least two general ways. First, the diffusional kurtosis can potentially be more sensitive to some tissue properties, such as heterogeneity, or as illustrated by the Kärger model, water exchange. Second, the diffusional kurtosis may be less sensitive to certain confounding effects and thereby serve as a more robust biomarker. One study, for example, has found that the MK in gray matter is altered substantially less by CSF contamination than either the MD or FA (70).

A few studies have already given encouraging, if very preliminary, results for the application of DKI to ischemic stroke (3,71,72), aging (42), Alzheimer's disease (73), schizophrenia (74), and attention deficit hyperactivity disorder (75). In addition, it has been shown that the extra information provided by DKI can be used to resolve intravoxel fiber crossings (38), which is not possible with DTI; as a consequence, DKI could be used to improve upon standard DTI-based fiber tracking.

Key advantages of DKI relative to other methods of quantifying diffusional non-Gaussianity are that its diffusion metrics are model independent and that it can be readily applied to clinical scanning. Q-space imaging methods can, in principle, calculate the same diffusion metrics as DKI, but the acquisition times and hardware requirements are substantially higher (32). In particular, q-space imaging methods typically utilize much larger maximum b-values than DKI. Multiple compartment models often provide a good fit to diffusion-weighted signal intensity data (16), but the interpretation of the model parameters may not always be clear (40). However, multiple compartment models are compatible with DKI and can be used to calculate the diffusional kurtosis as suggested by eqn (20). Stretched-exponential fits to diffusion-weighted signal intensity data (53), in contrast, are inconsistent with DKI and do not lead to meaningful kurtosis estimates.

CONCLUSION

DKI is a clinically feasible extension of DTI that allows for quantification of diffusional non-Gaussianity. With DKI, one obtains all the usual DTI diffusion metrics plus additional metrics related to the diffusional kurtosis. These new metrics can help to better characterize the water diffusion properties of brain tissue and, in particular, are sensitive to diffusional heterogeneity. Implementation of DKI is similar to DTI, except that at least 3 distinct b-values and 15 distinct diffusion directions are needed. A whole brain DKI data set with $3 \times 3 \times 3$ mm^3 isotropic voxels can be acquired with clinical 3T MRI scanners in less than 7 min.

Acknowledgements

We thank Els Fieremans, Mariana Lazar, Dmitry Novikov, Eric Sigmund, and Ali Tabesh for helpful discussions. The post-processing program utilized for this article was developed by Ali Tabesh. Caixia Hu assisted with data acquisition and analysis.

REFERENCES

1. Tanner JE, Stejskal EO. Restricted self-diffusion of protons in colloidal systems by the pulsed-gradient, spin-echo method. J. Chem. Phys. 1968; 49: 1768–1777.
2. DeCarlo LT. On the meaning and use of kurtosis. Psychol. Meth. 1997; 2: 292–307.
3. Jensen JH, Helpern JA. Quantifying non-Gaussian water diffusion by means of pulsed-field-gradient MRI. *Proceedings of the 11th Annual Meeting of ISMRM* Toronto, Canada 2003; 2154.
4. Jensen JH, Helpern JA, Ramani A, Lu H, Kaczynski K. Diffusional kurtosis imaging: the quantification of non-Gaussian water diffusion by means of magnetic resonance imaging. Magn. Reson. Med. 2005; 53: 1432–1440.
5. Lu H, Jensen JH, Ramani A, Helpern JA. Three-dimensional characterization of non-Gaussian water diffusion in humans using diffusion kurtosis imaging. Lu H, Jensen JH, Ramani A, Helpern JA. NMR Biomed. 2006; 19: 236–247.
6. Basser PJ, Mattiello J, Le Bihan D. Estimation of the effective self-diffusion tensor from the NMR spin echo. J. Magn. Reson. B. 1994; 103: 247–254.
7. Basser PJ, Mattiello J, Le Bihan D. MR Diffusion tensor spectroscopy and imaging. Biophys. J. 1994; 66: 259–267.
8. Basser PJ. Inferring microstructural features and the physiological state of tissues from diffusion-weighted images. NMR Biomed. 1995; 8: 333–344.

View this article online at wileyonlinelibrary.com Copyright © 2010 John Wiley & Sons, Ltd.

9. Basser PJ, Pierpaoli C. Microstructural and physiological features of tissues elucidated by quantitative-diffusion-tensor MRI. J. Magn. Reson. B. 1996; 111: 209–219.
10. Pierpaoli C, Jezzard P, Basser PJ, Barnett A, Di Chiro G. Diffusion tensor MR imaging of the human brain. Radiology. 1996; 201: 637–648.
11. Hui ES, Cheung MM, Qi L, Wu EX. Towards better MR characterization of neural tissues using directional diffusion kurtosis analysis. Neuroimage. 2008; 42: 122–134.
12. Lätt J, Nilsson M, Wirestam R, Johansson E, Larsson EM, Stahlberg F, Brockstedt S. In vivo visualization of displacement-distribution-derived parameters in q-space imaging. Magn. Reson. Imaging. 2008; 26: 77–87.
13. Duong TQ, Sehy JV, Yablonskiy DA, Snider BJ, Ackerman JJ, Neil JJ. Extracellular apparent diffusion in rat brain. Magn. Reson. Med. 2001; 45: 801–810.
14. Silva MD, Omae T, Helmer KG, Li F, Fisher M, Sotak CH. Separating changes in the intra- and extracellular water apparent diffusion coefficient following focal cerebral ischemia in the rat brain. Magn. Reson. Med. 2002; 48: 826–837.
15. van Pul C, Jennekens W, Nicolay K, Kopinga K, Wijn PF. Ischemia-induced ADC changes are larger than osmotically-induced ADC changes in a neonatal rat hippocampus model. Magn. Reson. Med. 2005; 53: 348–355.
16. Maier SE, Mulkern RV. Biexponential analysis of diffusion-related signal decay in normal human cortical and deep gray matter. Magn. Reson. Imaging. 2008; 26: 897–904.
17. Kärger J. Zur bestimmung der diffusion in einem zweibereichsystem mit hilfe von gepulsten feldgradienten. Ann. Phys. 1969; 479: 1–4.
18. Kärger J. NMR self-diffusion studies in heterogeneous systems. Adv. Colloid Interface Sci. 1985; 23: 129–148.
19. Kärger J, Pfeifer H, Heink W. Principles and applications of self-diffusion measurements by nuclear magnetic resonance. Adv. Magn. Reson. 1988; 12: 1–89.
20. Roth Y, Ocherashvilli A, Daniels D, Ruiz-Cabello J, Maier SE, Orenstein A, Mardor Y. Quantification of water compartmentation in cell suspensions by diffusion-weighted and T_2-weighted MRI. Magn. Reson. Imaging. 2008; 26: 88–102.
21. Lee JH, Springer CS Jr. Effects of equilibrium exchange on diffusion-weighted NMR signals: the diffusigraphic 'shutter-speed'. Magn. Reson. Med. 2003; 49: 450–458.
22. Cao J. Single molecule tracking of heterogeneous diffusion. Phys. Rev. E. 2001; 63: 041101.
23. Tanner JE. Transient diffusion in a system partitioned by permeable barriers. Application to NMR measurements with a pulsed field gradient. J. Chem. Phys. 1978; 69: 1748–1754.
24. Powles JG, Mallett MJD, Rickayzen G, Evans WAB. Exact analytic solutions for diffusion impeded by an infinite array of partially permeable barriers. Proc. R. Soc. London A-Math. Phys. Eng. Sci. 1992; 436: 391–403.
25. Sukstanskii AL, Yablonskiy DA, Ackerman JJ. Effects of permeable boundaries on the diffusion-attenuated MR signal: insights from a one-dimensional model. J. Magn. Reson. 2004; 170: 56–66.
26. Mitra PP, Sen PN, Schwartz LM, Le Doussal P. Diffusion propagator as a probe of the structure of porous media. Phys. Rev. Lett. 1992; 68: 3555–3558.
27. Latour LL, Svoboda K, Mitra PP, Sotak CH. Time-dependent diffusion of water in a biological model system. Proc. Natl. Acad. Sci. USA. 1994; 91: 1229–1233.
28. Novikov DS, Jensen JH, Helpern JA. Permeability and surface area of cell membranes from the DWI signal. *Proceedings of the 17th Annual Meeting of ISMRM* Honolulu, USA 2009; 451.
29. Crick F. Diffusion in embryogenesis. Nature. 1970; 225: 420–422.
30. Stejskal EO, Tanner JE. Spin diffusion measurements: spin echoes in the presence of a time-dependent field gradient. J. Chem. Phys. 1965; 42: 288–292.
31. Callaghan PT. *Principles of Nuclear Magnetic Resonance Microscopy*. Oxford University Press: Oxford, 1991.
32. Wedeen VJ, Hagmann P, Tseng WY, Reese TG, Weisskoff RM. Mapping complex tissue architecture with diffusion spectrum magnetic resonance imaging. Magn. Reson. Med. 2005; 54: 1377–1386.
33. Chabert S, Meca CC, Le Bihan D. Relevance of the information about the diffusion distribution in vivo given by kurtosis in q-space imaging. *Proceedings of the 12th Annual Meeting of ISMRM* Kytoto, Japan 2004; 1238.
34. Liu C, Bammer R, Acar B, Moseley ME. Characterizing non-Gaussian diffusion by using generalized diffusion tensors. Magn. Reson. Med. 2004; 51: 924–9937.
35. Mitra PP, Sen PN. Effects of microgeometry and surface relaxation on NMR pulsed-field-gradient experiments: Simple pore geometries. Phys. Rev. B. Condens. Matter. 1992; 45: 143–156.
36. Frøhlich AF, Ostergaard L, Kiselev VG. Effect of impermeable boundaries on diffusion-attenuated MR signal. J. Magn. Reson. 2006; 179: 223–233.
37. Jensen JH, Hu C, Helpern JA. Rapid data acquisition and post-processing for diffusional kurtosis imaging. *Proceedings of the 17th Annual Meeting of ISMRM* Honolulu, USA 2009; 1403.
38. Lazar M, Jensen JH, Xuan L, Helpern JA. Estimation of the orientation distribution function from diffusional kurtosis imaging. Magn. Reson. Med. 2008; 60: 774–7781.
39. Callaghan PT, Coy A, MacGowan D, Packer KJ, Zelaya FO. Diffraction-like effects in NMR diffusion studies of fluids in porous solids. Nature. 1991; 351: 467–469.
40. Kiselev VG, Il'yasov KA. Is the 'biexponential diffusion' biexponential? Magn. Reson. Med. 2007; 57: 464–469.
41. Umezawa E, Yoshikawa M, Yamaguchi K, Ueoku S, Tanaka E. Q-space imaging using small magnetic field gradient. Magn. Reson. Med. Sci. 2006; 5: 179–189.
42. Falangola MF, Jensen JH, Babb JS, Hu C, Castellanos FX, Di Martino A, Ferris SH, Helpern JA. Age-related non-Gaussian diffusion patterns in the prefrontal brain. J. Magn. Reson. Imaging 2008; 28: 1345–1350.
43. Hui ES, Cheung MM, Qi L, Wu EX. Advanced MR diffusion characterization of neural tissue using directional diffusion kurtosis analysis. Conf. Proc. IEEE Eng. Med. Biol. Soc. 2008; 3941–3944.
44. Cheung MM, Hui ES, Chan KC, Helpern JA, Qi L, Wu EX. Does diffusion kurtosis imaging lead to better neural tissue characterization? A rodent brain maturation study. Neuroimage. 2009; 45: 386–392.
45. Peled S, Whalen S, Jolesz FA, Golby AJ. High b-value apparent diffusion-weighted images from CURVE-ball DTI. J. Magn. Reson. Imaging. 2009; 30: 243–248.
46. Minati L, Aquino D, Rampoldi S, Papa S, Grisoli M, Bruzzone MG, Maccagnano E. Biexponential and diffusional kurtosis imaging, and generalised diffusion-tensor imaging (GDTI) with rank-4 tensors: a study in a group of healthy subjects. MAGMA. 2007; 20: 241–253.
47. Minati L. Rapid generation of biexponential and diffusional kurtosis maps using multi-layer perceptrons: a preliminary experience. MAGMA. 2008; 21: 299–305.
48. Lätt J, Nilsson M, Malmborg C, Rosquist H, Wirestam R, Ståhlberg F, Topgaard D, Brockstedt S. Accuracy of q-space related parameters in MRI: simulations and phantom measurements. IEEE Trans. Med. Imaging. 2007; 26: 1437–1447.
49. Yablonskiy DA, Bretthorst GL, Ackerman JJ. Statistical model for diffusion attenuated MR signal. Magn. Reson. Med. 2003; 50: 664–669.
50. Jespersen SN, Kroenke CD, Østergaard L, Ackerman JJ, Yablonskiy DA. Modeling dendrite density from magnetic resonance diffusion measurements. Neuroimage 2007; 34: 1473–1486.
51. Poot DHJ, den Dekker AJ, Sijbers J. Pearson set of distributions as improved signal model for diffusion kurtosis imaging. *Proceedings of the 17th Annual Meeting of ISMRM* Honolulu, USA 2009; 1393.
52. Jian B, Vemuri BC, Özarslan E, Carney PR, Mareci TH. A novel tensor distribution model for the diffusion-weighted MR signal. Neuroimage. 2007; 37: 164–1176.
53. Bennett KM, Schmainda KM, Bennett RT, Rowe DB, Lu H, Hyde JS. Characterization of continuously distributed cortical water diffusion rates with a stretched-exponential model. Magn. Reson. Med. 2003; 50: 727–734.
54. Poot DHJ, den Dekker AJ, Verhoye M, Blockx I, Van Audekerke J, Van Der Linden A, Sijbers J. Optimizing the diffusion weighting gradients for diffusion-kurtosis imaging *Proceedings of the 17th Annual Meeting of ISMRM* Honolulu, USA 2009; 1394.
55. Gallichan D, Scholz J, Bartsch A, Behrens TE, Robson MD, Miller KL. Addressing a systematic vibration artifact in diffusion-weighted MRI. Hum. Brain Mapp. 2010; 31: 193–202.
56. Carlson BC. Computing elliptic integrals by duplication. Numer. Math. 1979; 33: 1–1-16.
57. Press WH, Teukolsky SA, Vetterling WT, Flannery BP. *Numerical Recipes in C: The Art of Scientific Computing*. Cambridge University Press: New York, 1992; 261–271.
58. Qi LQ, Wang YJ, Wu EX. D-eigenvalues of diffusion kurtosis tensors. J. Comp. Appl. Math. 2008; 221: 150–157.
59. Qi LQ, Han DR, Wu EX. Principal invariants and inherent parameters of diffusion kurtosis tensors. J. Math. Anal. Appl. 2009; 349: 165–180.

Copyright © 2010 John Wiley & Sons, Ltd.

60. Sigmund EE, Lazar M, Jensen JH, Helpern JA. In vivo imaging of kurtosis tensor eigenvalues in the brain at 3 T. *Proceedings of the 17th Annual Meeting of ISMRM, Honolulu* USA 2009; 360.
61. Qin W, Yu CS, Zhang F, Du XY, Jiang H, Yan YX, Li KC. Effects of echo time on diffusion quantification of brain white matter at 1.5 T and 3.0 T. Magn. Reson. Med. 2009; 61: 755–760.
62. Dietrich O, Heiland S, Sartor K. Noise correction for the exact determination of apparent diffusion coefficients at low SNR. Magn. Reson. Med. 2001; 45: 448–453.
63. Le Bihan D, Breton E, Lallemand D, Aubin ML, Vignaud J, Laval-Jeantet M. Separation of diffusion and perfusion in intravoxel incoherent motion MR imaging. Radiology. 1988; 168: 497–505.
64. Maier SE, Bogner P, Bajzik G, Mamata H, Mamata Y, Repa I, Jolesz FA, Mulkern RV. Normal brain and brain tumor: multicomponent apparent diffusion coefficient line scan imaging. Radiology. 2001; 219: 842–849.
65. Maier SE, Mamata H, Mulkern RV. Characterization of normal brain and brain tumor pathology by chisquares parameter maps of diffusion-weighted image data. Eur. J. Radiol. 2003; 45: 199–207.
66. Le Bihan D, Mangin JF, Poupon C, Clark CA, Pappata S, Molko N, Chabriat H. Diffusion tensor imaging: concepts and applications. J. Magn. Reson. Imaging. 2001; 13: 534–546.
67. Sundgren PC, Dong Q, Gómez-Hassan D, Mukherji SK, Maly P, Welsh R. Diffusion tensor imaging of the brain: review of clinical applications. Neuroradiology. 2004; 46: 339–350.
68. Mori S, Zhang J. Principles of diffusion tensor imaging and its applications to basic neuroscience research. Neuron. 2006; 51: 527–539.
69. Alexander AL, Lee JE, Lazar M, Field AS. Diffusion tensor imaging of the brain. Neurotherapeutics 2007; 4: 316–329.
70. Hu C, Jensen JH, Falangola MF, Helpern JA. CSF partial volume effect for diffusional kurtosis imaging. *Proceedings of the 16th Annual Meeting of ISMRM* Toronto, Canada 2008; 3325.
71. Lätt J, van Westen D, Nilsson M, Wirestam R, Ståhlberg F, Holtås S, Brockstedt S. Diffusion time dependent kurtosis maps visualize ischemic lesions in stroke patients. *Proceedings of the 17th Annual Meeting of ISMRM* Honolulu, USA 2009; 40.
72. Helpern JA, Lo C, Hu C, Falangola MF, Rapalino O, Jensen JH. Diffusional kurtosis imaging in acute human stroke. *Proceedings of the 17th Annual Meeting of ISMRM* Honolulu, USA 2009; 3493.
73. Lu H, Jensen JH, Hu C, Falangola MF, Ramani A, Ferris S, Helpern JA. Alterations in cerebral microstructual integrity in normal aging and in Alzheimer's disease: a multi-contrast diffusion MRI study. *Proceedings of the 14th Annual Meeting of ISMRM* Seattle, USA 2006; 723.
74. Ramani A, Jensen JH, Szulc KU, Ali O, Hu C, Lu H, Brodie JD, Helpern JA. Assessment of abnormalities in the cerebral microstructure of schizophrenia patients: a diffusional kurtosis imaging study. *Proceedings of the 15th Annual Meeting of ISMRM* Berlin, Germany 2007; 648.
75. Helpern JA, Falangola MF, Di Martino A, Ramani A, Babb JS, Hu C, Jensen JH, Castellanos FX. Alterations in brain microstructure in ADHD by diffusional kurtosis imaging. *Proceedings of the 15th Annual Meeting of ISMRM* Berlin, Germany 2007; 1580.

View this article online at wileyonlinelibrary.com Copyright © 2010 John Wiley & Sons, Ltd.